CFD Modeling of TiO_2 Nano-Agglomerates Hydrodynamics in a Conical Fluidized Bed Unit with Experimental Validation

Bahramian, Ali Reza; Kalbasi, Mansour*+

Faculty of Chemical Engineering, Amirkabir University of Technology, Tehran, I.R. IRAN

ABSTRACT: *In the computational fluid dynamics (CFD) modeling of gas-solids two phase flow, the effect of boundary conditions play an important role in predicting the hydrodynamic characteristics of fluidized beds. In this work, the hydrodynamics of conical fluidized bed containing dried TiO_2 nano-agglomerates were studied both experimentally and computationally. The pressure drop was obtained by pressure measurements and mean solid velocity in the different axial and radial positions and their experimental values were measured by a parallel 3-fiber optical probe. The Eulerian-Eulerian multiphase model and granular kinetic theory with using Gidaspow (1994) drag function were applied in simulations. The effect of three different types of boundary conditions (BC) including no-slip/friction, free-slip/no-friction and high-slip/small-friction which were developed by Schaeffer (1987) and Johnson and Jackson (1987) were investigated. The results of the model were compared with the experimental data. The numerical simulation using free-slip/no-friction BC agreed reasonably well with the experimental pressure drop measurements. The pressure drops predicted by the simulations were in agreement with the experimental data at superficial gas velocities higher than the minimum fluidization velocity, U_{mf}. The results for simulated mean axial solid velocity showed that the free-slip/no-friction BC was in better agreement with the experimental data compared with other boundary conditions.*

KEY WORDS: *Conical fluidized bed, Computational fluid dynamics, Boundary condition, Numerical simulation, Fluidization, Hydrodynamic parameters, TiO_2 nano-agglomerates.*

INTRODUCTION

Fluidized and spouted beds are found in many plant operations, pharmaceutical, and mineral industries. A conical fluidized bed is a hybrid gas-particle contacting system; therefore, it has the characteristics of both fluidized and spouted beds. Naming of these beds in the literatures are often based on their geometrical shape and the ratio of the bed inlet diameter to the particle size diameter [1-4]. In some references, these systems are named as tapered fluidized bed [3, 4].

Conical fluidized beds provide means of good mixing

* To whom correspondence should be addressed.
+ E-mail: mkalbasi@aut.ac.ir
1021-9986/10/2/123 16/$/3.60

and circulation for particles of wide size distribution. Knowledge about hydrodynamics of gas and particle flow in conical fluidized bed is important to their design and required for both industrial applications and fundamental researches.

Mathur & Epstein [5]; and *Epstein & Grace* [6] have shown that the solid flow in a spouted bed could be divided into three regimes, each with its own specific flow behavior: the spout zone, in the center of the bed, the annular zone, between spout zone and the wall and the fountain located at the bed surface. In the spout zone the velocities of gas and particle phases are high while in the annular zone these values are low.

Kwauk [7] has reported that a decreasing fluid velocity gradient in the direction of fluid flow in a conical vessel has the following advantages:

(1) for poly-disperse solids, a higher velocity at the lower section of a cone provides adequate fluidization of the fine particles, while a lower velocity at the top section prevents excessive carry-over of the fines and nano-agglomerates.

(2) The highly agitated coarse particles in the lower zone serve as a normal gas distribution to disperse the fluidizing medium to the upper zone of the finer solids in the conical bed. Several theoretical studies and original correlations of gas and particle motions have been obtained for definite influence of size distribution on bed hydrodynamic such as increased bed expansion, decreased minimum fluidization velocity and smaller bubbles with more gas passing through the bed [1-2, 8-10].

The common experimental techniques used for the determination of trajectories, velocity and circulation of particles in the bed are: optical fiber [11-13], particle image velocimetry [14] and Laser Doppler Velocimetry (LDV) [15-16]. *He et al.* [12] used a fiber optic probe system to measure the vertical solid velocity profiles in the spout, annular and fountain zones of spouted bed. Radioactive particle tracking technique is used for the noninvasive measurement of the solid velocities along the walls of semi-column spouted beds and does not apply to conventional beds.

In the past two decades, due to the high performances of the computers and the advances made in the numerical techniques and computational fluid dynamics (CFD) tools have gained benefits [17-18]. The flow of gas and particle phases in the spout zone is dominated by gas turbulence and particle-particle collisions. Constitutive models for the stresses of particles in the spout zone can be deduced from the kinetic theory of granular flow by adapting the kinetic theory for granular flow. *Marschall & Mleczko* [19] performed a numerical investigation of a draft tube spouted bed of fine particles (200μm). These workers investigated the effects of inlet jet velocity on the pressure drop in the draft tube and particle residence time along the axis of the draft tube. A simplified Eulerian approach has been used where the interaction between phases was modeled with an empirical correlation. *Goldschmidt et al.* [20] employed a discrete particle model to predict particle motions in a pseudo-2D spout fluid bed. They also performed an experimental study in their system using optical measurement technique in order to validate their model. *Huilin et al.* [21] incorporated a kinetic-frictional constitutive model for dense assemblies of solids in the simulation of spouted beds. Their investigations showed the predicted solid velocities and volume fractions were in agreement with experimental observation of *He et al.* [12]. *Du et al.* [22] indicated that the *Gidaspow* [23] drag model gave the best agreement with experimental observation of *He et al.* [12]. This model used a form of the Ergun equation for its dense phase calculation to predict the gas and particle motion in a conical fluidized bed. *Wang et al.* [24] reported the flow behavior of agglomerates of nano-size particles in a spouted bed with an agglomerate-based approach. *Duarte et al.* [25] applied the Eulerian-Eulerian multiphase model for numerical simulation of fluid dynamics of spouted beds with two different geometries of conical-cylindrical and conical beds. The simulated pressure drop and minimum spouting condition were studied for different air flow rates. They obtained the results of CFD simulation a compared with the experimental values which were obtained through empirical correlations and show that the simulation results were in agreement with the experimental data. *Darelius et al.* [26] used a kinetic theory of granular flow and friction stress models using the slip and partial slip boundary conditions in their numerical simulation to predict the solid velocity at the wall region.

In this study, the experimental and numerical simulations were applied to predict the hydrodynamic behavior in a conical fluidized bed. The Eulerian-Eulerian multiphase model, including kinetic theory of granular flow and three different types of boundary

conditions including no-slip/friction, free-slip/no-friction and high-slip/small-friction, were investigated in numerical simulations. To validate the model, each boundary condition was compared with the experimental results obtained by using pressure measurements and the parallel 3-fiber optical probe technique.

THEORITICAL MODELS

In the two-fluid models, two sets of conservation equation are used for gas-solid phases. The reader should refer to Refs. [13,14] for the fundamental theoretical formulation of two-phase flow. Among the many models that have attempted to predict the hydrodynamics and the related characteristics of the fluidized and spouted beds, computational fluid dynamics (CFD) hold the greatest potential for long-term benefits [27]. CFD techniques are derived from the governing equations of the fluid flow in the form of partial differential equations (PDEs) representing the conservation of mass, momentum and energy. The governing equations can be summarized as follows:

The mass conservation equation for phase i (i=g, s) is:

$$\frac{\partial}{\partial t}\left(\alpha_i\rho_i\right)+\nabla\cdot\left(\alpha_i\rho_i\vec{v}_i\right)=0 \tag{1}$$

With the index *s* for solid phase and *g* for gas phase.

The momentum conservation equation for gas and solid phase is:

$$\frac{\partial}{\partial t}\left(\alpha_g\rho_g\vec{U}_g\right)+\nabla\cdot\left(\alpha_g\rho_g\vec{U}_g\vec{U}_g\right)= \tag{2}$$
$$-\alpha_g\nabla P+\nabla\cdot\bar{\bar{\tau}}_g-K_{gs}\left(\vec{U}_g-\vec{v}_g\right)+\alpha_g\rho_g\vec{g}$$

$$\frac{\partial}{\partial t}\left(\alpha_s\rho_s\vec{v}_s\right)+\nabla\cdot\left(\alpha_s\rho_s\vec{v}_s\vec{v}_s\right)= \tag{3}$$
$$-\alpha_s\nabla P+\nabla\cdot\bar{\bar{\tau}}_s-\nabla P_s+K_{gs}\left(\vec{U}_g-\vec{v}_s\right)+\alpha_s\rho_s\vec{g}$$

The granular temperature conservation for solid phase is given by:

$$\frac{3}{2}\left[\frac{\partial}{\partial t}\left(\alpha_s\rho_s\theta_s\right)+\nabla\cdot\left(\alpha_s\rho_s\theta_s\vec{v}_s\right)\right]= \tag{4}$$
$$-\left(P_s\bar{\bar{I}}+\alpha_s\bar{\bar{\tau}}_s\right):\nabla\cdot\vec{v}_s-\nabla\cdot\left(k_{\theta s}\nabla\theta_s\right)-\gamma\theta_s+\phi_{gs}$$

In these equations, K_{gs} is the fluid-particle interaction coefficient in drag model. This model is used from the *Ergun* [28] equation for dense phase calculation

$$\begin{cases}K_{gs}=150\dfrac{\alpha_s^2\mu_g}{\alpha_g d_s^2}+1.75\dfrac{\alpha_s\rho_g}{d_s}\left|\vec{v}_s-\vec{U}_g\right|\\ \alpha_g\le 0.8\end{cases} \tag{5}$$

and the *Wen & Yu* [29] equation for dilute phase calculation,

$$\begin{cases}K_{gs}=\dfrac{3}{4}C_D\dfrac{\alpha_s\alpha_g\rho_g\left|\vec{v}_s-\vec{U}_g\right|}{d_s}\cdot\alpha_g^{-2.65}\\ \alpha_g>0.8\end{cases} \tag{6}$$

where

$$\begin{cases}C_D=\dfrac{24}{Re_s}\left[1+0.15\left(Re_s\right)^{0.687}\right]\\ Re_s<1000\end{cases} \tag{7}$$

$$\begin{cases}C_D=0.44\\ Re_s\ge 1000\end{cases} \tag{8}$$

and relative Reynolds number

$$Re_s=\frac{\rho_g\cdot d_s\cdot\left|\vec{v}_s-\vec{U}_g\right|}{\mu_g} \tag{9}$$

To avoid the discontinuity of the two equations, *Gidaspow* [23] introduced a switch function that gave a rapid transition from one regime to the other:

$$\varphi_{gs}=\frac{\mathrm{Arc.tan}\left[150\times 1.75\left[0.2-\alpha_s\right]\right]}{\pi}+0.5 \tag{10}$$

Thus, the fluid-particle interaction coefficient can be expressed as

$$K_{gs}=\left(1-\phi_{gs}\right)K_{Ergun}+\phi_{gs}K_{Wen-Yu} \tag{11}$$

The value of fluid-solid exchange coefficient, K_{gs}, and restitution coefficient, e_{ss}, were chosen 1.0 and 0.9, respectively. Other constitutive equations are summarized in Table 1.

NUMERICAL SOLUTION

In the present numerical simulation an Eulerian-Eulerian multiphase model, including granular kinetic theory and k-ε turbulence model was used for both the solid and gas phases to simulate the hydrodynamic behavior

Table 1: Constitutive equations.

Solid stress-strain tensor $\overline{\tau}_s = \mu_s \left(\nabla \vec{v}_s + (\nabla \vec{v}_s)^T \right) + \left(\lambda_s - \frac{2}{3}\mu_s \right) \nabla . \vec{v}_s$
Solid shear viscosity $\mu_s = \mu_{s,kinetic} + \mu_{s,fr} + \mu_{s,col}$
Solid bulk viscosity $\lambda_s = \frac{4}{3}\varepsilon_s^2 \rho_s d_s g_{0,ss} (1+e_{ss}) \sqrt{\frac{\theta_s}{\pi}}$
Solid frictional viscosity $\mu_f = p_f \sin(\varphi) / 2\sqrt{I_{2D}}$
Collisional dissipation of energy $\gamma\theta_m = \frac{12(1-e_{ss}^2) g_{0,ss}}{d_p \sqrt{\pi}} \rho_s \alpha_s^2 \theta_s^{3/2}$
Solid pressure $P_s = \alpha_s \rho_s \theta_s + 2\rho_s (1+e_{ss}) \alpha_s^2 g_{0,ss} \theta_s$
Radial distribution function $g_{0,ss} = \left[1 - \left(\frac{\alpha_s}{\alpha_{s,Max}} \right)^{1/3} \right]^{-1}$
Granular energy diffusion coefficient $K\theta_s = \frac{150.\rho_s \sqrt{\theta_s . \pi}}{384.(1+e_{ss}).g_{0,ss}} . \left[1 + \frac{6}{5} . \alpha_s . g_{0,ss} . (1+e_{ss}) \right]^2$
Transfer of kinetic energy $\varphi_{gs} = -3K_{gs}\theta_s$

in a conical fluidized bed. The set of governing equations were solved by the finite control volume technique. The 2-Dimensional axisymmetric segregated solver was chosen in the simulations, since the conical fluidized bed was three-dimensional (3D); some differences between the numerical and experimental results were expected. However, *Du et al.* [30] reported a good qualitative agreement between 2D and 3D simulations of a gas-fluidized bed and indicated that 2D models could be used to reduce the computational time. The mesh used in the computation domain is shown in Fig. 2b. The computational grid was established and optimized to show the overall flow behavior within the vessel, while keeping the computational time at a reasonable level. Thus, while detailed information about the behavior of the fluid and the particles within the boundary layer can, in principle, be obtained by increasing the grid density near the wall boundary, this was not one of the current computational objectives of the model. The pressure-velocity coupling was obtained using the phase coupled SIMPLE algorithm (PC-SIMPLE). The PDEs are reduced to an approximate and equivalent set of algebraic equations, which are solved numerically to give the flow field at discrete points in the calculation domain. All partial differential equations were solved using a second order upwind discretization scheme; whereas the volume fraction equation was run with first order accuracy. The velocities were solved coupled with two phases in a segregated state. The pressure equation was built based on total volume continuity rather than mass continuity. Pressure and velocities were then corrected so as to satisfy the continuity constraint. The mesh density was chosen to fulfill the conditions for near-wall function and to minimize the solution's dependence on mesh density. The time step in unsteady simulations varied, depending on the solution convergence, between 5×10^{-5} to 1×10^{-3} s.

BOUNDARY CONDITIONS

The following assumptions and boundary conditions (BC) were applied in every simulation as follows:

1) Continuous phase was treated as ideal gas.

2) The axisymmetry boundary condition was applied along the axis of symmetry.

3) At the inlet boundary conditions, the inlet gas velocity was equal to the superficial gas velocity (from 0 m/s to 1.43m/s) and the inlet solid velocity was zero.

4) At the outlet, an out flow boundary condition was given, i.e., the velocity gradients for the two phase along the axial direction were zeros. Also, the pressure was specified (atmospheric condition).

5) At the wall, three different types of boundary conditions were assumed to description of the frictional stress. The gas tangential and normal velocities were set equal to zero (no-slip BC). The *Schaeffer* [31] approach was used for no-slip condition, while boundary semi-empirical equations developed by *Johnson & Jackson* [32] were applied for the tangential velocity and granular temperature of the solid phase for free- and high-slip conditions on the wall:

$$v_{s,w} = -B\frac{\partial v_{s,w}}{\partial n} \quad (12)$$

$$B = \frac{6\alpha_2 \cdot \mu_s}{\sqrt{3}\sqrt{\theta}\cdot\pi\cdot\varphi\cdot\rho_s g_{0,ss}} \quad (13)$$

Here φ is specularity coefficient and B is the slip coefficient. The granular temperature at walls, θ_w, was obtained in term of the collisional dissipation at the wall, γ_w, as:

$$\theta_w = -C_1\frac{\partial\theta_w}{\wp n} + C_2 \quad (14)$$

where

$$C_1 = \frac{k\theta_s}{\gamma_w}\ ;\ C_2 = \frac{\sqrt{3}\pi\rho_s u_{s,slip}^2 g_{0,ss}\theta_s^{3/2}}{6\alpha_{s,max}} \quad (15)$$

Where γ_w, was expressed in terms of wall restitution coefficient, e_w as:

$$\gamma_w = \frac{\sqrt{3}\left(1-e_w^2\right)\alpha_s\cdot g_{0,ss}\cdot\theta_s^{3/2}}{4\alpha_{s,max}} \quad (16)$$

The specularity coefficient is a measure of the fraction of collisions which transfer momentum to wall and varies from zero (free-slip condition) to one (no-slip condition). In fact, a high specularity coefficient is comparable to the large-friction limit, and a low specularity coefficient is similar to the small-friction limit. It is therefore easier to use the *Johnson & Jackson* [32] boundary condition and adjust the specularity coefficient to fit the experimental data. In order to assess the effect of boundary conditions on model, three simulations were run, employing three different boundary conditions for the solid phase, as described in Table 2. In the first simulation run (simulation run1), the no-slip BC with frictional effect of particles on the wall was employed. In the second simulation run (simulation run2), the free-slip BC without frictional effect of particles on the wall was used and finally in the third simulation run (simulation run3), the high-slip BC with small frictional effect of particles on the wall was used.

EXPERIMENTAL SETUP

The apparatus used in this work was a laboratory plexiglass conical fluidized bed (screen-bottomed type)

Table 2: Simulation performed at the this work.

Simulation runs	Friction	Slip condition
1	Friction	No-slip (φ=1)
2	No-friction	Free-slip (φ=0)
3	Small-friction	High-slip (φ=0.1)

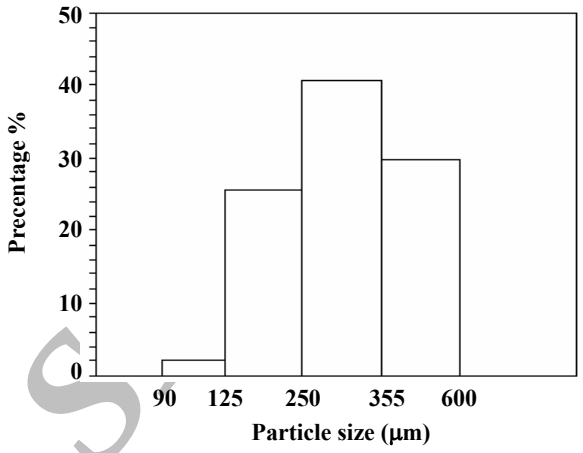

Fig. 1: Typical particle size distribution.

model STREA-1 (Aeromatic-Fielder, Bubendorf, Switzerland) with a stainless steel mesh of standard 60 mesh size at the base of vessel served to support the bed. Air (60 ^{oC}, 1 atm pressure) is used as spouting medium. Air flow was measured by a mass flow meter (Brooks, 5853 S), while pressure was measured by a differential pressure transducer (RS, 286-686). More details of the test procedure can be found in our last papers [33-34].

The particles used throughout this experiment were dried Titanium dioxide (TiO_2) nano-agglomerates with size distribution ranged between 90μm to 600μm (See particle size distribution curve in Fig. 1).

The mean agglomerate diameter equaled to 280 μm which was determined by the following equation:

$$d_p = 1\Big/\sum\left(x_i/d_{pi}\right) \quad (17)$$

In the above equation, x_i was percentage of the particle weight fraction in each range of particle diameter and d_{pi} stands for the mean particle diameter in the same range, which were determined by various meshes (90, 125, 250, 355 and 600 micron) and particles sieved according to the ISO 565 standard method.

The Schematic diagram of experimental setup as shown in Fig.2 and physical properties of materials and other information are set out in Table 3.

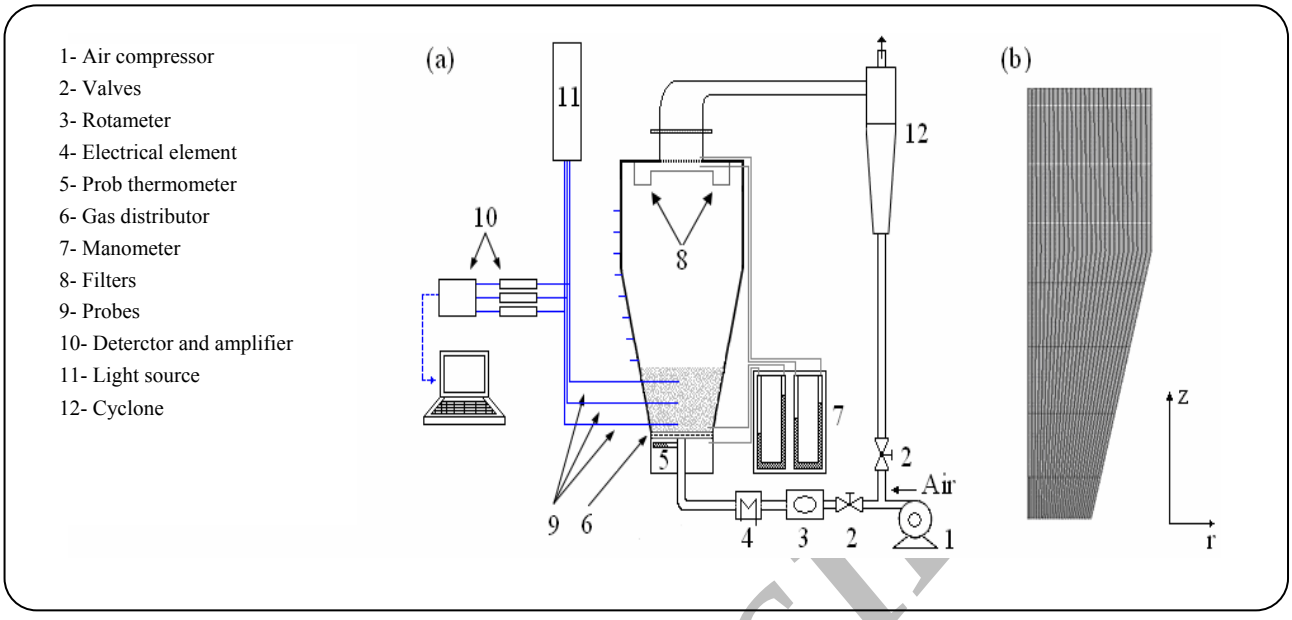

Fig. 2: (a) Schematic diagram of experimental setu; (b) Computational mesh (2D).

Table 3: Major parameters of the present experiments and simulations.

Parameter	Symbol	Experiments	Simulation
Type of particles used	TiO_2		
Mean particle diameter	d_p	280µm	280µm
Particle density	ρ_p	4500 (Kg/m^3)	Same
Bulk density	ρ_b	128.3 (Kg/m^3)	Same
Gas density	ρ_g	Air: 1.225 (Kg/m^3)	Same
Average gas pressure	P	6.5 MPa	Same
Superficial gas velocity	U_g	0 to 1.5m/s	0.1-1.43m/s
Static Bed height	H_o	0.061m	Same
Initial solid packing	$\alpha_{s,0}$	0.65	Same
Packing limit	$\alpha_{s,max}$	0.65	Same
Inlet column diameter	d_i	1.2×10^{-1}m	Same
Outlet column diameter	d_o	2.5×10^{-1}m	Same
Cone angle	γ	24 degree	Same
Total height of column	h	4.8×10^{-1}m	Same
Height of cylindrical part	h_{cyl}	1.8×10^{-1}m	Same
Height of conical part	h_{con}	3.0×10^{-1}m	Same
Outlet gas diameter	d_{og}	8×10^{-2}m	Same

Experimental analyses were performed to identify the steady state pressure drop, ΔP at different superficial gas velocities from 0 to 1.5 m/s. All of the experiments were performed with increasing the gas velocity from the fixed bed state to fully fluidized state and then decreasing gas velocity to reach the initial state. Time-mean pressure drop measurements were recorded at 10 Hz for 20s interval once steady-state conditions were achieved. The mean solid velocities in the different axial and radial positions were determined by a fiber-optic probe technique. When a particles circulates near the head of the probe, it reflects the light emitted by the central fiber. The frequency of the light was 50 Hz. The light signal was collected by photodiodes and converted into voltage (1-100 mV). The signals then was passed through the amplifier (-12 to +12V). A 12 V light source transmitted light to the emitting fiber, and a filter controlled the intensity of the beam. An analogue/digital interface sent the data to the computer for the processing. From the statistical analysis, by means of the cross-correlation function (incorporated in MATLAB 7.1 program), only those signals with statistically significant correlation coefficient are accepted. An r-z translator was used to position the probe set at desired coordinate location. It employed two stepper motors controlled through the GPIB port.

RESULTS AND DICUSSION

Fig. 3 show pressure drop evolution across the bed versus air inlet velocity. The air inlet velocity was gradually increased at regular time intervals to the maximum value and then air inlet velocity was decreased to 0m/s. the black points correspond to the experimental pressure drop obtained as air inlet velocity is increased, whereas the gray point corresponds to pressure drop values when air inlet velocity is decreased. The solid line is obtained numerically with CFD for increasing air inlet velocity and dashed line for decreasing it. This plot is usually called a characteristic curve [5]. The static bed height was selected to be 0.061m and the simulated characteristic curves for the above static bed height were determined through 8 simulations involving different gas spouting velocity by applying the *Gidaspow* [23] drag model.

As shown in Fig. 3, the simulated bed pressure drop decreased significantly at the beginning of the fluidization when the *Gidaspow* [23] drag model was applied.

Table 4: Simulated and experimental values of minimum spout velocity.

H_o(m)	U_{mf}			
	Exp.	Simulation		
		Run 1	Run 2	Run 3
0.061	0.232	0.214	0.221	0.217
Relative deviation (%)		7.76	4.76	6.46

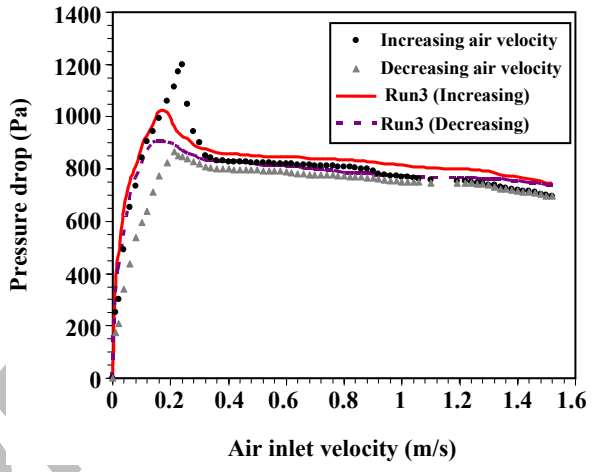

Fig. 3: Experimental data (Points) and simulated (lines) characteristic curves.

The relative deviation between the experimental and simulation results was 4.55% when free-slip/no-friction boundary condition was used.

It may be seen that the point where the spout collapsed and the bed pressure drop reduced suddenly, the gas velocity corresponded to the minimum fluidization which is the onset of fluidization of particles in the conical fluidized bed when particles start to move upward in the vessel. It was observed that due to the compact bed structure of dried fine TiO_2 particles and nano-agglomerates, the initial bed pressure drop was quite high for low gas flow rates. Increasing gas flow rate formed tiny cracks or channels in the bed, thus reducing the bed pressure drop. Table 4 shows the values of the minimum fluidization velocity obtained from experimental work and numerical simulations using CFD modeling. The results in table 3 indicated that the value of simulation run 2 was a minimum deviate from the experimental values, with a relative deviation of 4.76%.

It should be noted that a significant decrease in bed

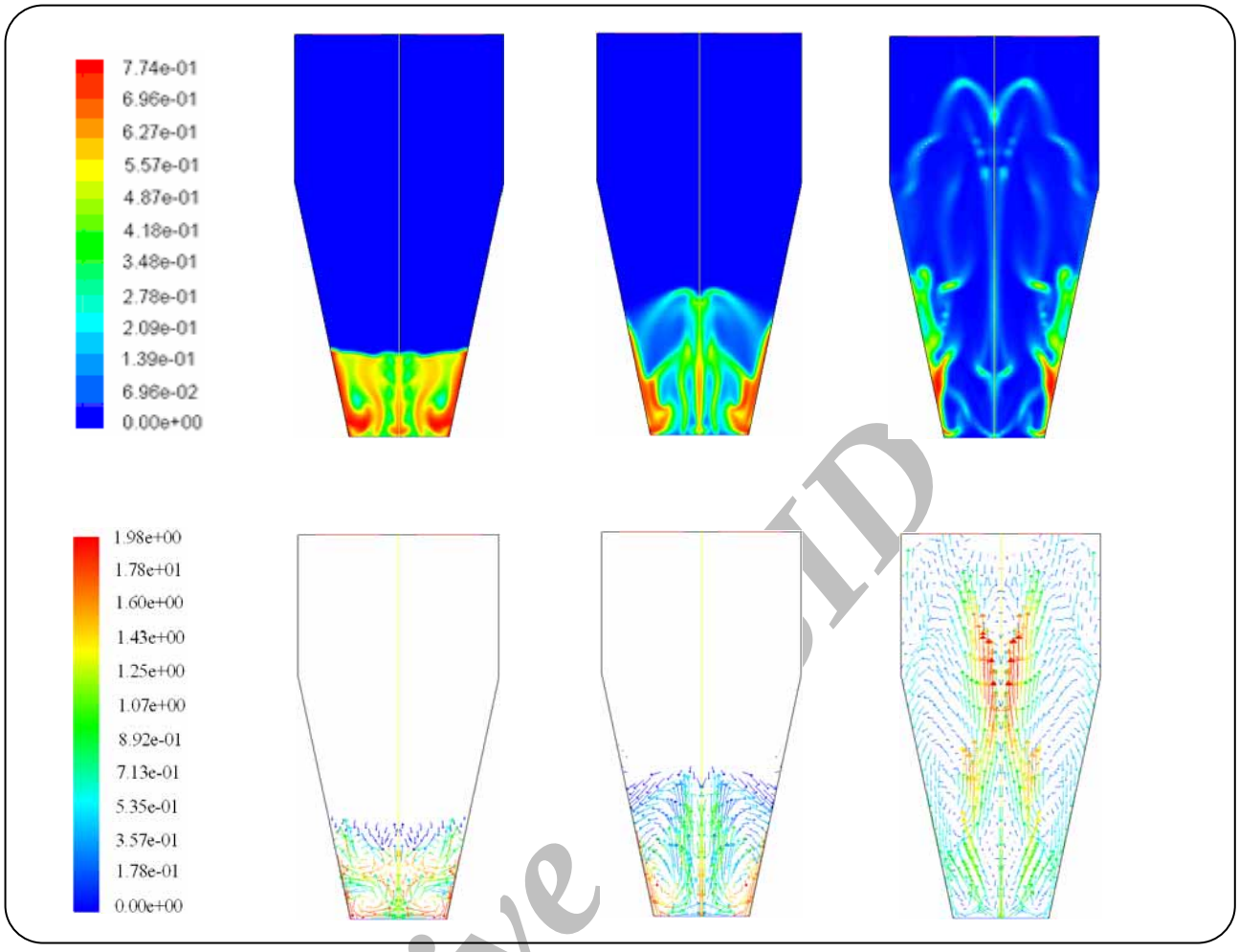

Fig. 4: simulated distribution of solids volume fraction profile in three gas velocity a: 1.43m/s, b: 0.7m/s and c: 0.1m/s (top) and their vectors of velocity (below)

pressure drop was observed before the full fluidization took place. The fluidization of fine TiO_2 in gas velocity range of 2-6×U_{ms} was homogenous. However, the full fluidization region resulted in the velocity range of about 3-6×U_{ms}. At the higher values of 3×U_{ms}, the experimental and simulated pressure drop values were close to each other. This result has also been obtained in spouted bed [25, 35]. The simulated time-averaged pressure drop was 3.5s.

Fig. 4 shows the simulated distribution of solids volume fraction profile in three gas velocity ranges of high (1.43m/s), medium (0.7m/s) and low (0.1m/s) and vector velocity of each contour according to run3. It was found from Fig. 4 that, in the spout zone the mean solid volume fraction are low while in the annular zone these values are high.

The description of the particle motion in the bed and base and close to the wall. This agreed with the visual also the estimated range of each zone (spout-annular and fountain) are shown in Fig. 5.

Particles are carried upwards by gas in the spout zone, reaching the top of the bed and form a fountain, and then drop down in the bed because of the gravity in the zone between the walls and the spout which namely is called the annular zone (Fig. 5). The experimental observations show that when the inlet gas velocity increases, the height of fountain distribution of particles increased and became more homogenous. The particles' motion in the spout, annular and fountain zones formed a circulation of particles in the bed called gulf-effect. The particles circulated toward the base of the vessel at positions near the wall were accelerated as they approached the base of the vessel, so that maximum velocity was attained at the

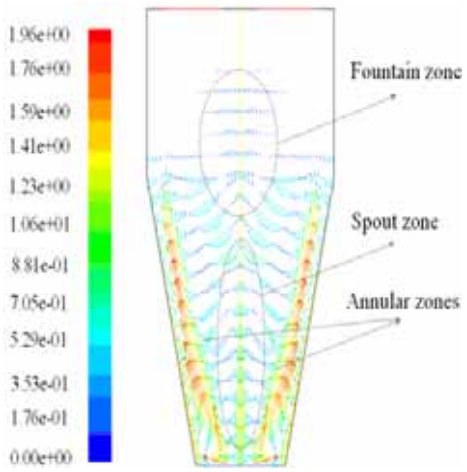

Fig. 5: Description of the particles motion in the bed.

observations made during the present work. Similar flow patterns of particles were found from both numerical simulations by *McKeen & Pugsley* [36]. They indicated that the computed solid velocity showed a gulf-effect with an upward flow in the central region and downward flow near the walls.

Figs. 6-9 indicates that the distribution of instantaneous velocity of solids for the *Gidaspow* [23] drag model with the inlet gas velocities of 0.10, 0.5, 0.9 and 1.43m/s which correspond to 0.42, 2.1, 3.78 and $6U_{mf}$, was examined at the time 3.5s after the gas was introduced to the bed. Fig. 6 corresponds to gas velocity below the minimum fluidization velocity, whereas Fig. 7 to Fig. 9 correspond to gas velocity above the minimum fluidization velocity.

Fig. 10 shows the experimental and simulated mean axial solid velocity distribution as a function of bed axial distance at different inlet gas velocity. As shown in Fig. 10a the experimental mean axial solid velocity accelerated to its maximum velocity between values of 0.62m/s to 0.91m/s, for inlet air velocity of 0.5 to 1.43m/s, respectively. It can be see that from Fig. 10a, at the gas velocities equal to 0.5m/s, the particles were rapidly increased to their maximum velocity (U=0.48m/s) at a height of about 0.06-0.07m and then the mean axial solid velocity decreased to zero at a height of about 0.19m from the vessel. Also, at the gas velocities equal to 1.43m/s, the particles were rapidly increased to their maximum velocity (U=0.9m/s) at a height of about 0.16m and at a higher height, the mean axial solid velocity decreased to zero at about 0.37m**.** Therefore the experimental results showed that by increasing the inlet gas velocity, the mean solid velocity increased and consequently the particles ascended to the upper heights in the vessel. As a result, by enhancing the inlet gas velocity, the expanded bed height increased.

Figs. 10b-d show the effect of the three different boundary conditions on the axial solid velocity profiles for the *Gidaspow* [23] drag model. The Figs. 10b-d also shows that by increasing the gas velocity, the height of the expanded bed increased. This agreed with the experimental data of Fig. 7a. Within the three boundary conditions chosen for simulation, the results showed that, when using a free-slip boundary condition (Fig. 10c), it was clear that the mean axial solid velocity was in a better agreement with the experimental results, while by using a no- or high-slip boundary conditions according to the simulation run1 and 3 (Figs. 10b & 10d), it was in less agreement with the experimental results. According to the results of mean solid velocity (Fig. 10b-d), at the inlet section a low accuracy between the experimental and simulation results was obtained. This may be due to the inaccurate modeling of the inlet configuration and conditions which can not be implemented in the model unless the simulation of the complete 3-D geometry was conducted.

Fig. 11 indicates the radial profile curves for experimental and simulated mean axial solid velocity at different heights with gas velocity of 1.43m/s. The velocities of the particles have their maxima in the spout zone (approximate zone $-0.05<r/R<0.05$) and gradually decrease in the annular zone (approximate zones between $r/R\leq-0.28$ and $r/R\geq0.28$). The velocities of particles approached to zero at a position that corresponded to the spout and annular zones, so called spout-annulus interface.

As shown in Fig. 11, the simulated solid velocity using *Gidaspow* [23] drag model (Fig. 11b-d) gave the closest results compared with the experimental solid velocity data (Fig. 11a).

It can be observed that particles flow up in the spout zone (positive solid velocity values) and flow down in the annular zone (negative solid velocity values). The mean axial solid velocity varied from the maximum in the center of the bed, gradually decreased, and finally reached a minimum near the walls. These results were consistent with other works in the literature [12, 21, 37].

In the inlet condition (the height between the 0.05 to 0.2m in Fig. 11), it can be see that the solid velocity

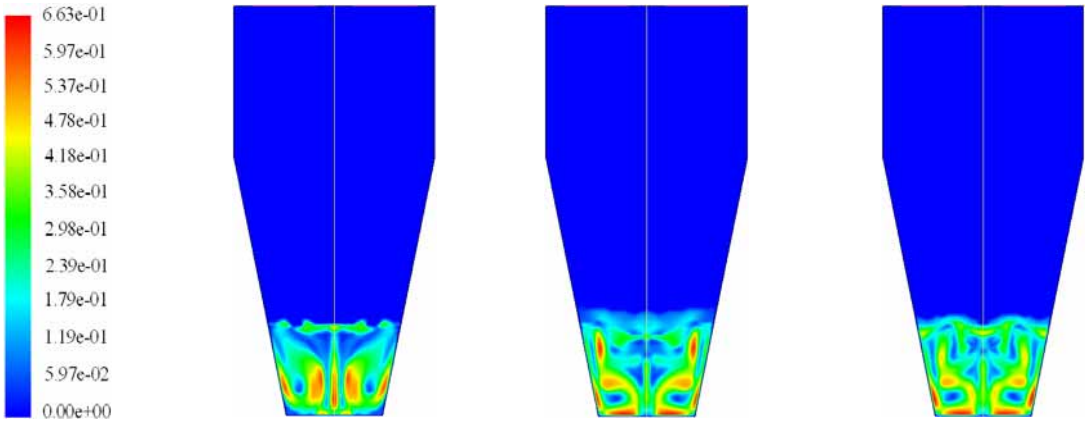

Fig. 6: Simulated distribution of solids velocity profile with an inlet gas velocity of 0.1m/s (a: no-slip BC; b: Free-slip/no-friction BC and c: High-slip/Small-friction BC).

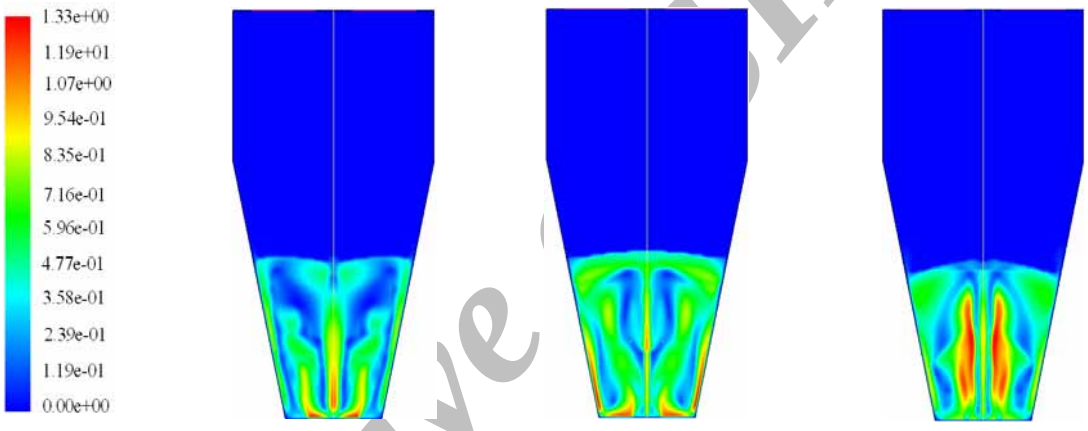

Fig. 7: Simulated distribution of solids velocity profile with an inlet gas velocity of 0.5m/s (a: no-slip BC; b: Free-slip/no-friction BC and c: High-slip/Small-friction BC).

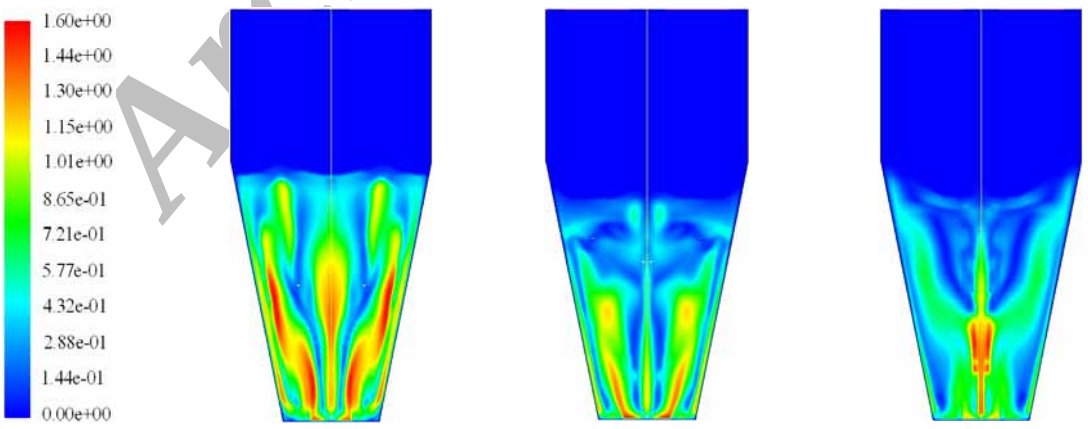

Fig. 8: Simulated distribution of solids velocity profile with an inlet gas velocity of 0.9m/s (a: no-slip BC; b: Free-slip/no-friction BC and c: High-slip/Small-friction BC).

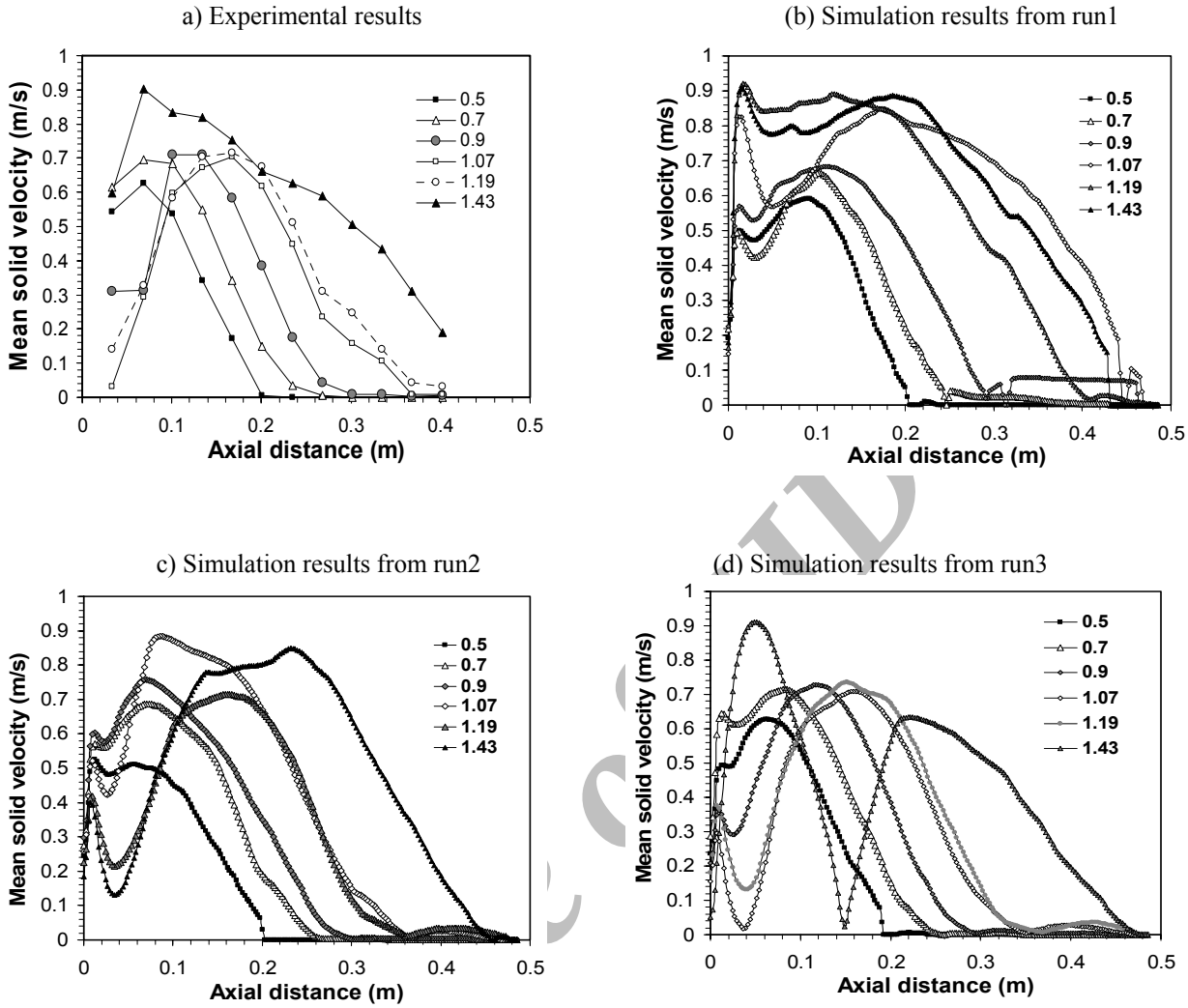

Fig. 10: Variation of mean axial solid velocity along the axis.

profile in both spout and annular zones was very pronounced, while the solid velocities in both zones became flatter at the higher bed height (0.3 to 0.485m). Meanwhile, it was observed from the experimental results that the mean axial solid velocity was a maximum value at z=0.1m at velocity about 1.18m/s while these values for simulation run1, 2, and 3 were about 1.16, 1.19 and 1.12m/s, respectively. It can be seen that when z=0.4m, the value of mean solid velocity for experimental results was about 0.16m/s, and for simulation results from run1, 2, and 3 were about 0.14, 0.17, and 0.12m/s.

Considering a very small friction or no friction limits, the solid velocity was slightly over-predicted. This was due to the physical behavior of the particle-wall interactions which was close to the free-slip boundary condition. Table 5 shows the relative deviation between the experimental and simulation results of the mean solid velocity in the axial (Fig. 11) and dimensionless radial (Fig. 11) positions.

Figs. 12-14 shows the radial profile curves of simulated mean axial solid velocity as a function of gas velocity at height of 0.05 and 0.3m in the conical fluidized bed. It may be noticed that the particles flow upwards in the spout, and downwards in the annular zone. The mean axial solid velocity varied from the maximum in the spout zone and gradually decreases to reach a minimum in the spout-annular interface. The mean axial solid velocity also increased in both the spout and the annular zones with increasing the gas velocity.

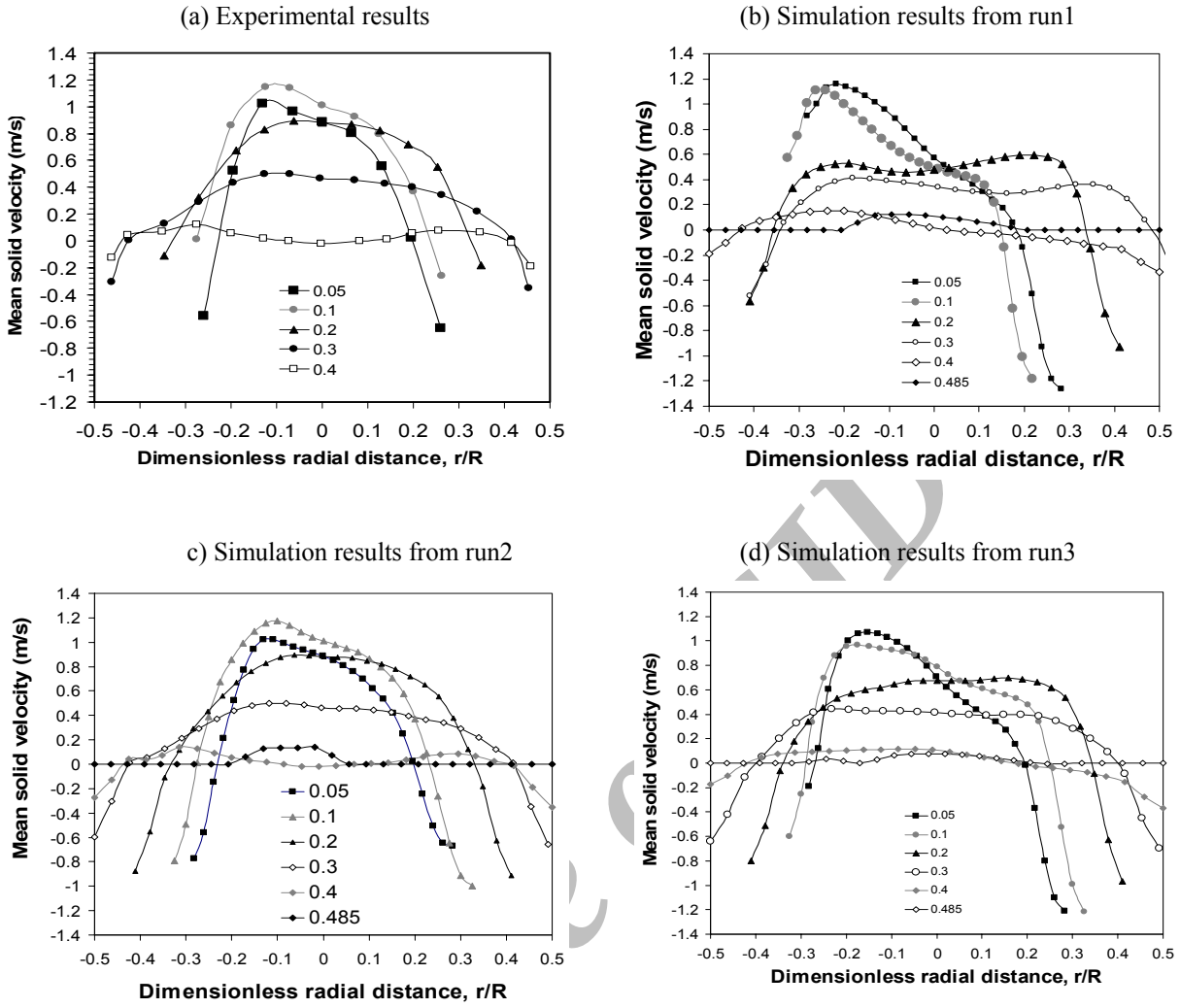

Fig. 11: Profile of mean axial solid velocity as a function of bed height.

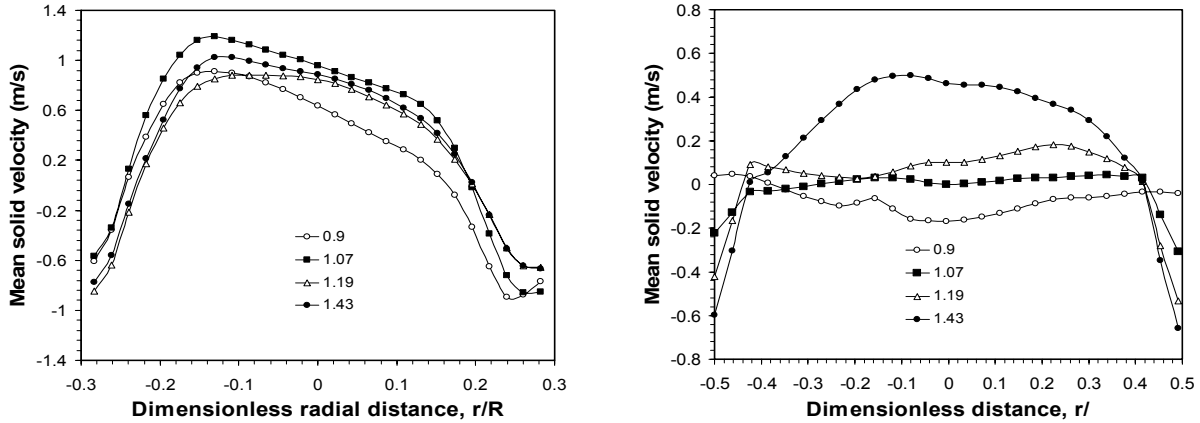

Fig. 12: Profile of mean solid velocity as a function of gas velocity for simulation run1, a) H=0.05m; b) H= 0.3m.

Table 5: Relative deviation between the experimental and simulation results for mean axial solid velocity (%).

Simulation	Axial position	Dimensionless radial position	
		Spout zone	Annular zone
Run 1	7.08	7.83	6.18
Run 2	3.47	2.97	2.02
Run 3	6.14	4.71	3.73

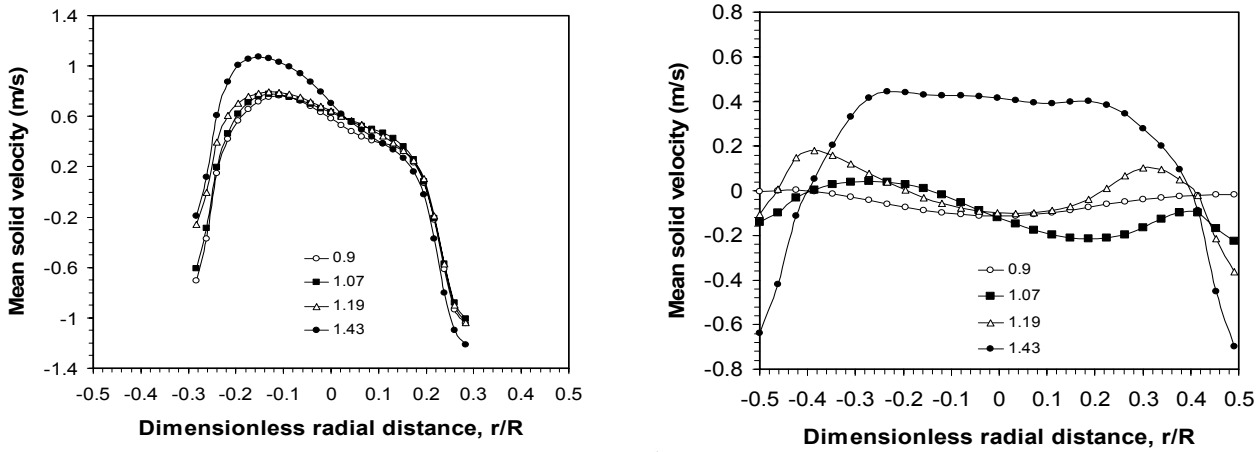

Fig. 13: Profile of mean solid velocity as a function of gas velocity for simulation run2, a) H=0.05m; b) H= 0.3m

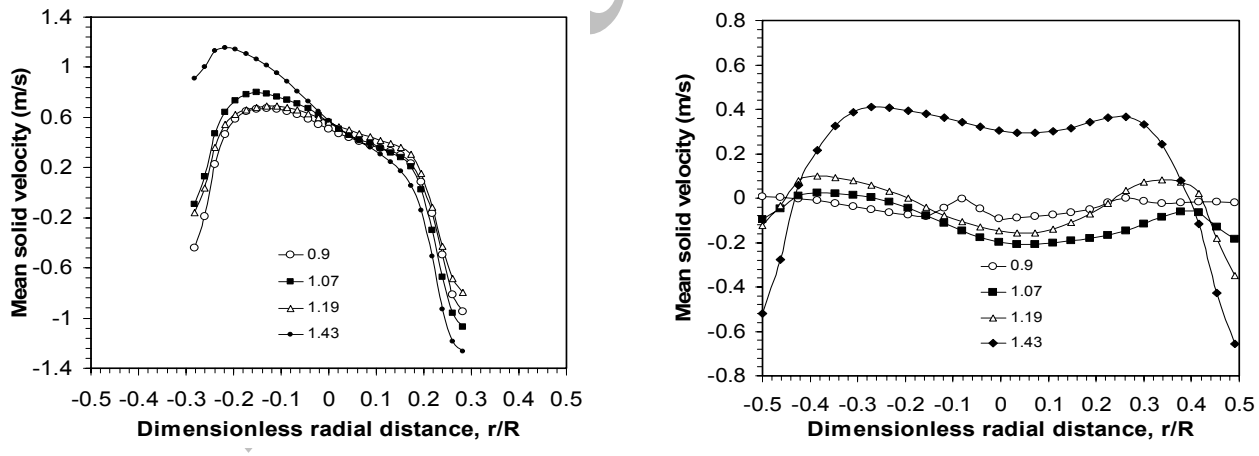

Fig. 14: Profile of mean solid velocity as a function of gas velocity for simulation run3, a) H=0.05m; b) H=0.3m.

High gas velocity increased the gas flux, and thus the velocity of particles in the spout. The velocity of particles was also increased in the annulus to balance the mass flux of solids between the spout and annulus. Hence, the high gas velocity increased the mixing of particles between spout and annulus zones in the conical fluidized bed.

CONCLUSIONS

The effects of three different types of boundary conditions consisted of no-slip/friction, free-slip/ no-friction and high-slip/small-friction were investigated to predict the hydrodynamic characteristics of conical fluidized bed and the results of numerical simulation

were validated by experimental work. The dried TiO_2 particles were used in experimental work and numerical simulation. The Eulerian-Eulerian multiphase model, involving granular kinetic theory was applied to the analysis and prediction of the hydrodynamics of a conical fluidized bed. The methodology used in numerical simulations for each types of boundary condition was validated by comparison with experimental data. According to the experiments, the bed pressure drop was enhanced with increasing the gas velocity from zero to a maximum value and then decreased as the gas velocity further increased. The minimum fluidization velocity, U_{mf}, was determined by relation between the differential bed pressure drop and gas velocity. The experimental velocity profiles for the solid phase in different axial and radial positions were obtained by using a parallel 3-fiber optical probe. The simulation results showed a better agreement with the experimental data at velocities above U_{mf}. The minimum fluidizatin velocity value simulated by using a free-slip/no-friction boundary condition showed a 4.55% deviation with respect to the experimental data. The minimum standard deviation for radial curves between the experimental and simulated results for mean axial solid velocity was 2.02% by applying free-slip/no-friction boundary condition. The value of mean axial solid velocity near the wall also better agreed with the experimental data. The simulation results like the experimental observation showed the spout, annular and fountain zones and particle circulation in the bed. Here the behavior of conical fluidized bed is similar to the spouted beds. The gas velocity had a distinct effect on the particle velocity in the spouting zone but had little effect on the particle velocity in the annular region. This agreed with the experimental data obtained and was in good agreement with the numerical results.

Acknowledgments

The authors would like to thank the Laser and Optic Research School (AEOI) for optical experiments and digital analysis and mechanical engineering department of Amirkabir University of Technology for digital analysis and equipments.

Numencluture

Symbols

B	Slip coefficient, dimensionless
C_D	Drag coefficient
d_i	Inlet diameter, m
e_{ss}	Restitution coefficient, dimensionless
g	Acceleration due to gravity, m/s^2
$g_{0,ss}$	Radial distribution coefficient, dimensionless
h	Total height of column, m
H	Height, m
H_o	Static bed height, m
$\bar{\bar{I}}$	Stress tensor, dimensionless
I_{2D}	Second invariant of the deviatoric stress tensor, dimensionless
K	Turbulent kinetic energy, kg/ms^3
$k\theta_s$	Diffusion coefficient for granular energy, kg/ms
K_{sg}	Momentum interphase exchange coefficient, dimensionless
P	Pressure, Pa
p_f	Frictional stress, dimensionless
R,r	Radius, m
Re	Reynolds number, dimensionless
T	Time, s
U,u	Velocity, m/s
v	Velocity, m/s
z	Height from the bottom of the vessel

Greek letters

α_i	Volume fraction, dimensionless
α_I	Loose bed volume fraction, dimensionless
$\gamma\theta_m$	Collision dissipation of energy, kg/ms^3
γ	Cone angle
θ_I	Granular temperature, m^2/s^2
λ_I	Bulk viscosity, kg/ms
μ_I	Shear viscosity, kg/ms
ν_I	Kinematic viscosity, m^2/s
ρ_I	Density, kg/m^3
$\bar{\bar{\tau}}_i$	Stress tensor, Pa
ϕ_{gs}	Transfer rate of kinetic energy, kg/ms^3
φ	Specularity coefficient, dimensionless.

Subscripts

b	Bulk
con	Conical
cyl	Cylindrical
g	Gas
i	General index
mf	Minimum fluidization
o	Outlet

p	Particle
q	Phase
s	Solids
t	Terminal (e.g. vt is the terminal velocity)
w	Wall

Received : Dec. 9, 2008 ; Accepted : Jun. 9, 2009

REFERENCES

[1] Tanfara H., Pugsley T., Winters C.C., Effect of Particle Size Distribution on Local Voidage in a Bench-Scale Conical Fluidized Bed Dryer, *Drying Technology*, **20**, p. 1237 (2002)

[2] Wang T., Wang J., Yang W., Jin. Y., Experimental Study on Bubble Behavior in Gas-Liquid-Solid Three-Phase Circulating Fluidized Beds., *Powder Technology*, **137**, p. 83 (2003).

[3] Chen Y., Wu R., Mori S., Development of a New Type of Thermogravimetric Analyzer with a Mini-Tapered Fluidized Bed. Effect of Fluidization of Particles on the Stability of the System, *Chem. Energy. J.*, **68**, p. 7 (1997).

[4] Shi Y.-F., Yu, Y.S., Fan L.T., Incipient Fluidization Condition for a Tapered Fluidized Bed, *Ind. Chem. Fundam*., **23**, p. 484 (1984).

[5] Mathur K.B., Epstein N., "Spouted beds", Academic Press, Inc LTD., New York, 304 pp. (1974).

[6] Epstein N., Grace J.R., "Spouting of particulate solids", In: Fayed, M.E., Otten, L. (EDs.), "Handbook of power Sci. & Technol.", (Chap.10) second ed. Chapman& Hall, New York (1997)

[7] Kwauk, M., "Fluidization- Idealized and bubbleless with applications, "Science Press and Ellis". Horwood, Beijing, 91 (1992)

[8] Yates J.G., Newton D., Fine Particle Effects in a Fluidized Bed Reactor, *Chem. Eng. Sci*., **41**, p. 801 (1986)

[9] Grace J.R., Sun G., Influence of Particle Size Distribution on the Performance of Fluidized Bed Reactors, *Can J. Chem. Eng.*, **69**, p. 1126 (1991).

[10] Khoe G.K., Ip T.l., Grace J.R., Rheological and Fluidization Behavior of Powders of Different Particle Size Distribution, *Powder Technology*, **66**, p. 127 (1990)

[11] Olazar M., San Jose M.J., Lamosas R., Alvarez S., Bilbao J., Study of Local Properties in Conical Spouted Beds Using an Optical Fiber Probe, *Ind. Eng. Chem. Research*, **34**, p. 4033 (1995).

[12] He Y.L., Qin S.Z., Lim C.J., Grace J.R., Particle Velocity Profiles and Solid Flow Patterns in Spouted Beds, *Can. J. Chem. Eng.*, **72**, p. 561 (1994b).

[13] Olazar M., San Jose M.J., Izquierdo M.A., Ortiz de Salazar A., Bilbao J., Effect of Operating Conditions on Solid Velocity in the Spout, Annulus and Fountain of Spouted Beds, *Chem. Eng. Sci*., **56**, p. 3585 (2001).

[14] Link J., Zeilstra C., Deen N., Kuipers H., Validation of a Discrete Particle Model in a 2D Spouted-Fluid Bed Using Non-Intrusive Optical Measuring Techniques, *Can. Chem. Eng.*, **82**, p. 30 (2004).

[15] Darelius A., Lennartsson E., Rasmuson A., Niklasson Bjorn I., Folestad S., Measurements of the Velocity Field and Frictional Properties of Wet Masses in a High Shear Mixer, *Chem. Eng. Sci.*, **62**, p. 2366 (2007a).

[16] Valverde J.M., Quintanilla M.A.S., Castellanos A., Lepek D., Quevedo J., Dave R.N., Pfeffer R., Fluidization of Fine and Ultrafine Particles Using Nitrogen and Neon as Fluidizing Jases, *AIChE J*., **54**, p. 86 (2008).

[17] Patankar V., "Numerical heat transfer and fluid flow", Hemisphere publishing company, (1980).

[18] Wilcox D.C., "Turbulence Modeling for CFD", (Third ed), Hardcover, Nov. 1, (2006).

[19] Marschall K.J., Mleczko L., CFD Modeling of an Internally Circulating Fluidized Bed Reactor, *Chem. Eng. Sci*., **64**, p. 2085 (1999).

[20] Goldschmidt M.J.V., Kuipers J.A.M., Van Swaaij W.P.N., Hydrodynamic Modeling of Dense Gas-Fluidized Beds Using the Kinetic Theory of Granular Flow: Effect of Coefficient of Restitution on Bed Dynamics, *Chem. Eng. Sci*., **56**, p. 571 (2001).

[21] Huilin L., Yurong H., Wentie L., Ding J., Gidaspow D., Bouillard J., Computer Simulations of Gas-Solid Flow in Spouted Bed Using Kinetic-Frictional Stress Model of Granular flow, *Chem. Eng. Sci*., **59**, p. 865 (2004).

[22] Du W., Bao X., Xu J., Wei W., "Computational Fluid Dynamics (CFD) Modeling of Spouted Bed: Influence of Frictional Stress, Maximum Packing Limit and Coefficient of Restitution of Particles". *Chem. Eng. Sci.*, **61**, p. 4558 (2006).

[23] Gidaspow D., "Multiphase Flow and Fluidization", Academic Press, Boston, (1994).
[24] Wang S.Y., He Y.R., Lu H.L., Zheng J.X., Liu G.D., Ding Y.L., Numerical Simulations of Flow Behavior of Agglomerates of Nano-Size Particles in Bubbling and Spouted Beds with an Agglomerate-Based Approach, *Trans IChemE, Part C*, **85**, (2007).
[25] Duarte C.R., Olazar M., Murata V.V., Barrozo M.A.S., Numerical Simulation and Experimental Study of Fluid-Particle Flows in a Spouted Bed, *Powder Technol*., Available Online 3 May (2008).
[26] Darelius A., Rasmuson VanWachem B., Bjorn I.N., Folestad S., CFD Simulation of the High Shear Mixing Process Using Kinetic Theory of Granular Flow and Frictional Stress Models, *Chem. Eng. Sci*., **63**, 2188 (2008).
[27] Fan R., O. Fox R.O., Segregation in Polydisperse Fluidized Beds: Validation of a Multi-Fluid Model, *Chem. Eng. Sci*., **63**, p. 272 (2008).
[28] Ergun S., Fluid Flow Through Packed Columns, *Chem. Eng. Progress*, **48**, p. 89 (1952).
[29] Wen C.Y., Yu Y.H., Mechanics of Fluidization, *Chem. Eng. Sci. Prog*., **62**, p. 100 (1966).
[30] Du W., Bao X., Xu J., Wei W., Computational Fluid Dynamics (CFD) Modeling of Spouted Bed: Assessment of Drag Coefficient Correlations, *Chem. Eng. Sci*., **61**, p. 1401 (2006)
[31] Schaeffer D.G., Instability in the Evolution Equations Describing Incompressible Granular Flow, *J. Diff. Eq*. **66**, p. 19 (1987).
[32] Johnson P.C., Jackson R., Frictional-Collisional Constitutive Relations for Granular Materials, with Application to Plane Shearing, *J. Fluid Mech*., **176**, p. 67 (1987).
[33] Kalbasi M., Bahramian A., Khorshidi J., Prediction of Minimum Spout Velocity and Moisture Distribution of Amonim Perchlorate Particles in a Spouted Bed Dryer, Iranian, *J. Chem. & Chem. Eng*., **26**, p. 113 (2007).
[34] Kalbasi M., Bahramian A., *Proceeding of International Workshop and Symposium on Industrial Drying*-, 20-23rd December, Mumbai, India. (2004)
[35] Taghipour F., Ellis N., Wong C., Experimental and Computational Study of Gas-Solid Fluidized Bed Hydrodynamics, *Chem. Eng. Sci*., **60**, 6857 (2005).
[36] McKeen T., Pugsley T., Simulation and Experimental Validation of a Freely Bubbling Bed of FCC Catalyst, *Powder Technol*., **129**, P.139 (2003).
[37] Kmiec A., Hydrodynamics of Flow and Heat Transfer in Spouted Beds, *Chem. Eng. J*., **19**, p. 189 (1980).